Hydrodynamical description of long-wavelength density fluctuations of helium in wedges

E. S. Hernández
Departamento de Física, Facultad de Ciencias Exactas y Naturales, Universidad de Buenos Aires, 1428 Buenos Aires, Argentina and Consejo Nacional de Investigaciones Científicas y Técnicas, Buenos Aires, Argentina
(Received 7 August 2009; published 21 January 2010)

The hydrodynamical model that has proven successful to describe excitations of superfluid helium in the bulk and adsorbed on planar surfaces, cylinders, and spheres is applied to investigate the long-wavelength density fluctuation spectrum of ^{4}He confined to an infinite linear wedge at zero temperature. It is found that in spite of the breaking of axial symmetry, the velocity potentials and the shape of the meniscus can be described in terms of an orbital quantum number or quasiangular momentum, and that the density wave spectrum is formally similar to that of helium shells adsorbed in a cylindrical pore. As an illustration, the stability of phonon and ripplon modes are discussed in terms of the relevant parameters of helium in a cesium wedge.

DOI: 10.1103/PhysRevB.81.024514 PACS number(s): 05.30.Jp, 68.08.Bc

I. INTRODUCTION

Fluids confined among walls of various shapes, such as pores, cavities, wedges and slits, have attracted the interest of researchers of several fields, as this topic encompasses disciplines such as the physics of adsorption and wetting with varying geometric parameters that define the form of the substrate and the confining potential, the thermodynamics of finite samples of matter, and the collective excitations of these samples. In particular, the physics of fluids in wedges received substantial attention,[1–14] originating descriptions of wedge wetting based on thermodynamics and statistical mechanics,[2,4,13] variational procedures that minimize the total surface free energy of the liquid-vapor interface[1,3,5] and applications of density-functional theory to the three-dimensional trapped fluid.[14] The series of papers that focus on the phase transitions undergone by the adsorbed liquid[6–8,10,12] have illuminated the role of fluctuations in the critical behavior of fluids in wedges. Specially, the connection between wetting and capillary condensation has been clarified by examining fluid adsorption in power-law wedges and by establishing the existence of a clear geometry-dominated regime.[9]

In a recent work,[14] density-functional theory calculations of the structure and energetics of superfluid ^{4}He in planar infinite wedges brought to light several interesting aspects of the adsorption of nanoscopic fluid samples, at zero temperature. In particular, it has been shown that in addition to the well-known filling transition, which occurs as the liquid-vapor interface becomes flat, an "emptying" transition preannouncing the formation of a bridge can take place for sufficiently narrow openings. Furthermore, the study of the adsorbed density profiles and their energetics has provided a reference frame for more involved analysis of the adsorption isotherms of helium in infinite pores[15] and on nanostructured surfaces.[16]

Since these studies concentrate on the equilibrium properties of the confined fluid, it is natural to take one step forward and interrogate oneself about the low-energy collective excitations supported by such systems. Accordingly, the purpose of the present work is to investigate the spectrum of density fluctuations of macroscopic amounts of helium in an infinite linear wedge of opening 2α. The theoretical frame to evaluate this spectrum is quantum fluid hydrodynamics, that has proven to be a trustworthy instrument to describe capillarity waves and density fluctuations in helium films adsorbed in the interior of cylindrical pores,[17] on planar surfaces[17] and on spherical substrates.[18] As shown in this work, this method permits a systematic analysis of the excitation spectrum as a function of the linear density of adsorbed atoms and wedge aperture, identifying the quantum numbers in the absence of cylindrical symmetry, as well as the detection of the regions of stability of phonon and ripplonlike propagation modes.

This paper is organized as follows. Section II contains the discussion of the wedge geometry and of the adequate coordinate systems. The hydrodynamic description is reviewed in Sec. III and the proposed solutions are developed in detail for the various meniscus shapes, together with some numerical illustrations. This work is summarized in Sec. V.

II. GEOMETRY OF THE FLUID CONFINED IN A WEDGE

The morphology of a macroscopic fluid sample with constant density ρ_0 confined to a linear wedge at bulk equilibrium has been derived in Ref. 5 and can be summarized as follows. Assuming that the total area of the transverse section—alternatively, the total number of particles per unit length along the wedge axis, here denoted by y—is a prescribed constant, the free energy of the system is minimized for an interfacial shape $f(x)$ that corresponds to a circumference of radius R in the (x,z) plane perpendicular to the wedge axis. According to the relationship between the contact angle θ_c and the wedge half-opening α, the following possibilities appear:

$$\theta_c < \tfrac{\pi}{2} - \alpha, \quad \text{circular concave meniscus},$$

$$\theta_c = \tfrac{\pi}{2} - \alpha, \quad \text{planar meniscus},$$

$$\tfrac{\pi}{2} + \alpha \geq \theta_c > \tfrac{\pi}{2} - \alpha, \quad \text{circular convex meniscus},$$

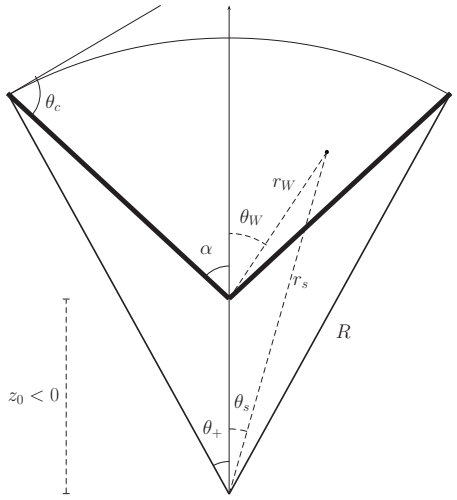

FIG. 1. Transverse section of the fluid sample in a linear wedge with a convex meniscus. The thick lines indicate the walls at half-opening α; the circular interface of radius R forms an angle θ_c with the solid wall. The center of the free surface lies at (negative) z_0 below the wedge vertex, and θ_1 is the angle of the contact line as viewed from that center.

$$\theta_c > \tfrac{\pi}{2} + \alpha, \quad \text{circular bridge},$$

where the crossover between curvatures at $\theta_c = \frac{\pi}{2} - \alpha$ corresponds to the so-called filling transition. The shape of systems with convex and concave meniscus and a circular bridge are, respectively, portrayed in Figs. 1–3. The geometrical parameters are related as follows. If $n = N/L$ is the number of adsorbed particles per unit length along the y axis, let $A = n/\rho_0$ be the area of the sample on the (x,z) plane. Then one has

$$R = \frac{\sqrt{A}}{\sqrt{\theta_c + \alpha - \frac{\pi}{2} + \frac{\cos\,\theta_c \cos(\theta_c + \alpha)}{\sin\,\alpha}}}, \tag{1}$$

$$z_0 = -R\frac{\cos\,\theta_c}{\sin\,\alpha}\text{sign}\left(\theta_c + \alpha - \frac{\pi}{2}\right), \tag{2}$$

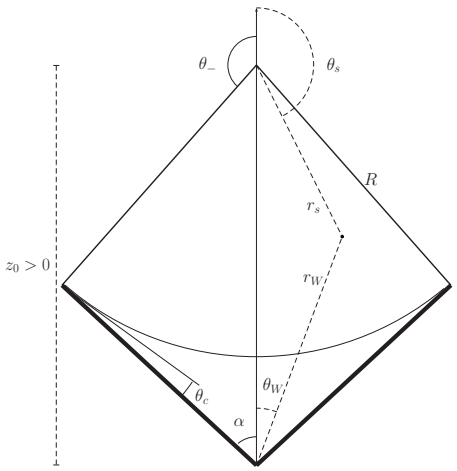

FIG. 2. Same as Fig. 1 for a concave meniscus.

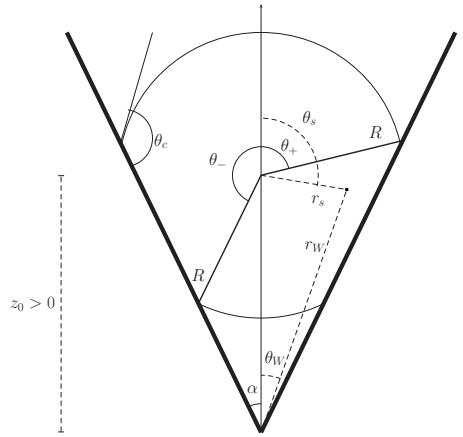

FIG. 3. Same as Figs. 1 and 2 for the bridge shape.

$$\theta_+ = \theta_c + \alpha - \frac{\pi}{2}, \quad \text{convex meniscus and bridge}, \tag{3}$$

$$\theta_- = \theta_c + \alpha + \frac{\pi}{2}, \quad \text{concave meniscus}, \tag{4}$$

$$= -\theta_c + \alpha + \frac{3\pi}{2}, \quad \text{bridge}. \tag{5}$$

Furthermore, it is important for future reference to note that there are two alternative systems of polar coordinates, respectively, referred to the wall (r_w, θ_w) and to the free surface (r_s, θ_s), both shown in Figs. 1–3, mutually related as

$$r_w = \sqrt{r_s^2 + z_0^2 + 2r_s z_0 \cos\,\theta_s}, \tag{6}$$

$$r_s = \sqrt{r_w^2 + z_0^2 - 2r_w z_0 \cos\,\theta_w}, \tag{7}$$

$$r_w \sin\,\theta_w = r_s \sin\,\theta_s, \tag{8}$$

$$r_w \cos\,\theta_w = r_s \cos\,\theta_s + z_0. \tag{9}$$

Figure 4 displays the different meniscii in the plane (θ_c, α), where the separatrices $\theta_c = \pi/2 \pm \alpha$ are plotted. One can visualize the sequence of transitions (a) for fixed wedge opening and varying contact angle and (b) for fixed contact angle and varying aperture. In forthcoming sections I shall focus on sequence (b) for the average contact angle of helium on planar Cs, $\theta_c = 36°$ (see, i.e., Ref. 19 for a review on experimental data and theoretical computations of θ_c).

III. HYDRODYNAMIC APPROXIMATION: CAPILLARY AND DENSITY WAVES FOR THE DIFFERENT MENISCUS SHAPES

Capillary waves in spherical fluid drops and cavities are analyzed in textbooks[20,21] and the derivation of hydrodynamic density waves of helium films in the interior of cylindrical pores has been carried out in Ref. 17. A model for a helium system adsorbed on a spherical substrate of radius R, as a shell of density ρ_0 surrounding the sphere up to a sharp

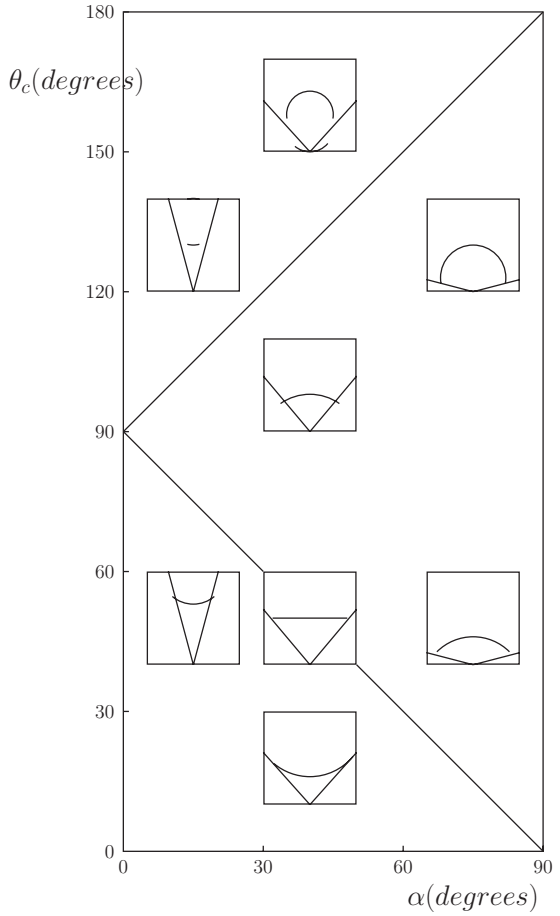

FIG. 4. Sequences of meniscii shapes in the (θ_c, α) plane. The oblique lines correspond to the separatrices $\theta_c = \pi/2 \pm \alpha$. The columns display sequences (a) varying contact angle at fixed wedge opening, the rows display sequence (b) fixed contact angle and varying aperture.

radius a has been presented in Ref. 18. In this theoretical frame, one derives the mode spectrum starting from the linearized continuity and momentum conservation equations for superfluid flow,

$$\frac{\partial \rho}{\partial t} = -\rho_0 \nabla \cdot \mathbf{v}_s, \tag{10}$$

$$m\rho_0 \frac{\partial \mathbf{v}_s}{\partial t} = -\nabla P - \rho_0 \nabla U \tag{11}$$

with ρ_0 the bulk density, $\mathbf{v}_s$ the superfluid velocity, P the pressure across the liquid-vapor interface, and $U(\mathbf{r})$ the external potential on a single helium atom of mass m.

A central issue in the construction of the spectrum are the boundary conditions (bc's). For the wedge geometry, these correspond to: (a) vanishing of the velocity normal to either wall at angle $\pm\alpha$ with the z axis, i.e., $\mathbf{v}_s \cdot \hat{n}_w = 0$; (b) on the free surface that corresponds to the meniscus of the helium sample, one has $\mathbf{v}_s \cdot \hat{n}_s = \partial\eta/\partial t$.

Here $\hat{n}_w$ and $\hat{n}_s$ are unit vectors perpendicular to the corresponding surface. The system for the wave equation with the given bc's consists then of

$$\nabla^2 \varphi + \frac{\omega^2}{c_s^2}\varphi = 0, \tag{12}$$

$$\mathbf{v}_s \cdot \hat{n}_w = 0, \tag{13}$$

$$\left[\frac{1}{m}\nabla U \cdot \hat{n}_s + K_1\right] \nabla \varphi \cdot \hat{n}_s|_R = \omega^2 \varphi|_R \tag{14}$$

with c_s the sound velocity in bulk helium and K_1 the excess curvature in the cylindrical geometry[17]

$$K_1 = \frac{1}{R^2} + \frac{1}{R^2}\frac{\partial^2}{\partial \theta_s^2} + \frac{\partial^2}{\partial y^2} \tag{15}$$

being R the radius of the circular cross-section in Figs. 1–3.

As in Ref. 17, one look for solutions of the wave equation of the form $\varphi(r,\theta,y) = \varphi(r,\theta)e^{iky}$. Equation (12) then becomes

$$(\nabla_{r,\theta}^2 + q^2)\varphi = 0 \tag{16}$$

with $q^2 = \omega/c_s^2 - k^2$. Capillary waves of incompressible fluid systems are obtained solving Laplace's equation $\nabla\varphi = (\nabla_{r,\theta}^2 - k^2)\varphi = 0$ for the velocity potential with the corresponding bc's. If propagation of density fluctuations is allowed, i.e., if the fluid is compressible with finite c_s one seeks perturbations $\delta\rho(r)$ proportional to the solution $\varphi(r)$ of the wave equation, together with a dispersion relation $\omega = c_s q$. In the long-wavelength limit $qR \ll 1$, expansion of the proposed potential up to second order in q^2 leads to the eigenfrequencies ω by solving Eq. (14).

A variational estimate of the eigenvalues has been presented in Ref. 22. The procedure in the current geometry consists of assuming perturbations of the meniscus shape $\eta(\theta_s, y, t) = r_s(\theta_s, y, t) - R$ of the form

$$\eta(\theta_s, y, t) = \varepsilon f(\theta_s) e^{i(ky - \omega t)} \tag{17}$$

with ε a small amplitude parameter, and looking for a velocity potential

$$\varphi(r_s, \theta_s, y, t) = -i\omega\varepsilon\Phi(r_s, \theta_s)e^{i(ky-\omega t)}. \tag{18}$$

The superfluid velocity $d\eta/dt$ is the gradient of φ if and only if

$$f(\theta_s) = \left.\frac{\partial \Phi(r_s, \theta_s)}{\partial r_s}\right|_R. \tag{19}$$

Then if $\mathcal{O}$ is the operator on the left-hand side of Eq. (14), this bc can be stated as

$$\mathcal{O} f(\theta_s) = \omega^2 \Phi(R, \theta_s) \tag{20}$$

from where the variational estimate for the convex (+) and concave (−) meniscii follows as:

$$\omega_{\pm}^2 = \frac{\int_{-\theta_{\pm}}^{\theta_{\pm}} d\theta_s f(\theta_s)[\mathcal{O} f(\theta_s)]}{\int_{-\theta_{\pm}}^{\theta_{\pm}} d\theta_s f(\theta_s)\Phi(\theta_s)}. \tag{21}$$

In order to establish the velocity potential, one should notice that the bc at the wall is naturally expressed in the wedge coordinates as $\partial\Phi/\partial\theta_w|_\alpha = 0$. For planar, concave, and

convex meniscii the wave Eq. (12) is satisfied with the given bc by

$$\Phi_\lambda(r_w,\theta_w) = J_\lambda(qr_w)\cos\lambda\theta_w \tag{22}$$

with $\lambda = l\pi/\alpha$, $l=0,\pm 1,\ldots$ and J_λ a cylindrical Bessel function, regular at $r_w=0$. Now the surface bc is most naturally accomplished by functions of the form

$$\Phi_\nu(r_s,\theta_s) = [J_\nu(qr_s) + B_\nu N_\nu(qr_s)]e^{i\nu\theta_s} \tag{23}$$

with $\nu = n\pi/\theta_\pm$, $n=0,\pm 1,\ldots$ and with N_ν the cylindrical Bessel function singular at $r_s=0$. To ensure that the wedge vertex is a stagnation point, one must choose $B_\nu = -J'_\nu(q|z_0|)/N'_\nu(q|z_0|)$, which sets the quantization rule for the surface momentum q. Note that positive q^2 corresponds to phonons and $q^2=-\kappa^2<0$ to ripplons. In the last case the velocity potential is expressed in terms of the modified Bessel functions $I_\nu(\kappa r_s)$ and $K_\nu(\kappa r_s)$ in Eq. (22) and $I_\lambda(\kappa r_w)$ in Eq. (21).

Analytical and numerical estimates are simpler in the wedge system, where the substrate potential is computed as $U(r_w,\theta_w)$. In these coordinates the shapes of the convex and concave meniscii are, respectively, described by

$$R_\pm(\theta_w) = z_0\cos\theta_w \pm \sqrt{R^2 - z_0^2\sin^2\theta_w}. \tag{24}$$

The radial derivative on the corresponding free surface and the operator $\mathcal{O}$ are then constructed taking into account Eqs. (6)–(9) and using chain rules. Focusing on the propagation velocities in the long-wavelength limit, one must consider the stability of the modes. For this sake, it is sufficient to consider $\Phi_\lambda = r_w^\lambda\cos\lambda\theta_w$ and carry the necessary operations. In this case, the integer l and the real λ, respectively, play the role of an orbital quantum number and of a quasiangular momentum and can be employed to assign a multipolarity to the modes in the wedge system.

While some significant results are discussed in Sec. IV, for the sake of completeness two important cases are mentioned here. One is the bridge shape; in this case, since the origin of coordinates in the wedge system does not belong to the fluid sample, the radial factor in the velocity potential should be chosen as $J_\lambda(qr_w)+AN_\lambda(qr_w)$. The constant A is in charge of coupling the two surfaces and is determined by equating the eigenvalue, Eq. (40), in the upper and lower meniscii, the respective shapes being described by Eq. (24). Note that for liquid ^{4}He in a Cs wedge, such configuration cannot occur in macroscopic samples. The other situation is that of a planar meniscus. In this case the height Z and base X of the triangular cross-section of the fluid are geometrically established and one sets $\eta(x,y,t)=z(x,y,t)-Z$. The formulation in Eqs. (17)–(40) is easily restated and the outcome is presented below.

IV. RESULTS IN THE LONG-WAVELENGTH LIMIT

In this section the long-wavelength limit $qR \ll 1$ is considered. The first case of interest which can be examined analytically to some extent involves the monopole modes. For a single curved meniscus this corresponds to a velocity potential for phonon ($q^2>0$) propagation

$$\Phi_0(r_w) = 1 \pm \frac{1}{4}q^2r_w^2 = 1 - \frac{1}{4}q^2(r_s^2 + z_0^2 + 2r_sz_0\cos\theta_s) \tag{25}$$

with the shape perturbation

$$f_0(\theta_s) = -\frac{q^2}{2}(R + z_0\cos\theta_s). \tag{26}$$

Moreover, it is necessary to analyze the concave and convex meniscii distinctly, due to the different sign of the outwards normal $\hat{n}_s$ and of the excess curvature. The surface bc is then

$$\pm\left(\left.\frac{\partial U(r_s,\theta_s)}{\partial r_s}\right|_R + \frac{\sigma k^2}{m\rho_0}\right)f_0(\theta_s) - \frac{\sigma}{2m\rho_0 R}q^2 = \omega_0^2\Phi_0(R,\theta_s) \tag{27}$$

with the $\pm$ sign for the convex and the concave surfaces, respectively. Using this sign convention, it is convenient to introduce the average gravity

$$g_\pm = \frac{1}{A}\int_{-\theta_\pm}^{\theta_\pm} d\theta_s \frac{1}{m}\left.\frac{\partial U(r_s,\theta_s)}{\partial r_s}\right|_R (R + z_0\cos\theta_s)^2. \tag{28}$$

The variational estimate, Eq. (40), thus gives up to lowest order in q^2R^2

$$\omega_0^2 = c_{R\pm}^2q^2,$$

$$= \frac{c_{R\pm}^2c_s^2}{c_{R\pm}^2 - c_s^2}k^2 \tag{29}$$

with the intrinsic first sound velocity and gravity

$$c_{R\pm}^2 = \frac{R}{4}(\mp g_\pm + g_{R\pm}), \tag{30}$$

$$g_{R\pm} = \frac{2\sigma}{m\rho_0R^2} \equiv g_\pm\left(\frac{a_\pm}{R}\right)^2 \tag{31}$$

in terms of the capillary length $a_\pm = \sqrt{2\sigma/(\rho_0 m g_\pm)}$. Accordingly, phonons are stable provided that $g_+ < -(4c_s^2 + g_{R+})$ and $g_- > (4c_s^2 + g_{R-})$ on the corresponding interface. Although values $c_{R\pm}^2<0$, fulfilled for $g_+ > -g_{R+}$ and $g_- < g_{R-}$ yield a positive prefactor in front of k^2 in the second line of Eq. (29), this would lead to an unstable radial mode.

Third sound (ripplon) propagation may take place if $\kappa^2 = -q^2 < 0$. In this case, the dispersion relation takes the form

$$\omega_0^2 = -c_{R\pm}^2\kappa^2 \tag{32}$$

that leads to the same form in Eq. (29) for $\omega^2(k)$. Clearly, the phonon and ripplon radial oscillations cannot be simultaneously stable; for predominantly attractive substrate forces, $g_\pm$ is positive and phonons are damped away on a convex meniscus. Instead, first sound is allowed in concave interfaces below the gravity threshold $4c_s^2 + g_{R-}$. The stability regions are displayed in Fig. 5. These results mirror those obtained in Ref. 17 for modes in a cylindrical pore, keeping in mind that the above variational estimate encompasses the breaking of polar symmetry.

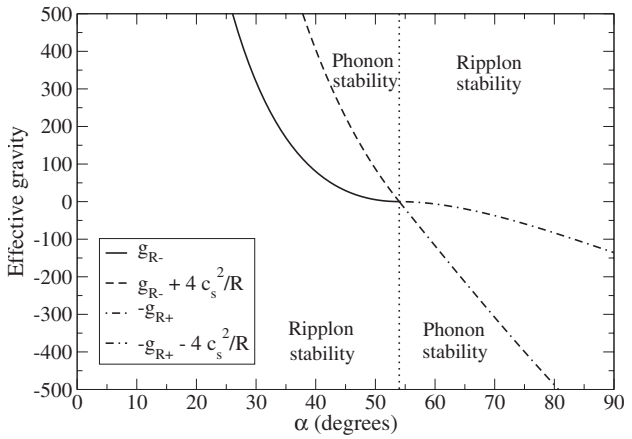

FIG. 5. The stability regimes for the monopole oscillation as a function of wedge opening. The effective gravity thresholds indicated by the four curves are qualitative and displayed in arbitrary units. The vertical line indicates the filling transition for ^{4}He in a Cs wedge. The unlabeled regions correspond to unstable regimes for either type of oscillation.

For a flat meniscus at the filling transition, R is infinite and one can keep the overall structure so far displayed with a shape profile

$$f_0^{flat} = \left.\frac{\partial \Phi_0(x,z)}{\partial z}\right|_Z = -\frac{q^2}{2}Z \tag{33}$$

a curvature operator equal to $-\partial^2/\partial x^2$, and gravity

$$g = \frac{1}{2mX}\int_{-X}^{X} dx \left.\frac{\partial U(x,z)}{\partial z}\right|_Z [f_0^{flat}]^2. \tag{34}$$

Letting $c_\infty^2 = Zg/2$, the result is

$$\omega_0^2 = -c_\infty^2 q^2 \quad \text{for phonons}, \tag{35}$$

$$= c_\infty^2 \kappa^2 \quad \text{for ripplons}, \tag{36}$$

$$= \frac{c_\infty^2 c_s^2}{c_\infty^2 + c_s^2} k^2 \tag{37}$$

showing once again that first sound cannot be supported in the vertical direction in the presence of positive gravity.

For nonvanishing multipolarity and a single curved surface, one has

$$\Phi_\lambda(r_w, \theta_w) = r_w^\lambda \cos\theta_w, \tag{38}$$

$$f_\lambda(\theta_w) = \frac{\lambda}{R}[R_\pm^\lambda \cos\lambda\theta_w - z_0 R_\pm^{\lambda-1}\cos(\lambda-1)\theta_w],$$

$$= \frac{\lambda}{R} R_\pm^{\lambda-1}\cos\lambda\theta_w[\pm\sqrt{R^2 - z_0^2\sin^2\theta_w} - z_0 \sin\lambda\theta_w \sin\theta_w], \tag{39}$$

where the meniscus radius is that of Eq. (23). After some algebra, the dispersion relation can be expressed, regardless the sign of q^2, as

$$\omega_{\lambda\pm}^2(k) = \frac{\lambda}{R}\left[g_\pm + \frac{\sigma}{m\rho_0 R^2}(1-k^2R^2)\mathcal{N}_\pm - \frac{\sigma}{m\rho_0 R^2}\langle l^2\rangle_\pm\right], \tag{40}$$

(cf. Ref. 17) where

$$g_\pm = \frac{R}{\lambda}\frac{\int_{-\alpha}^{\alpha} d\theta_w \frac{1}{m}\left.\frac{\partial U(r_w,\theta_w)}{\partial r_s}\right|_R [f(\theta_w)]^2}{\int_{-\alpha}^{\alpha} d\theta_s f(\theta_w)\Phi(R,\theta_w)}, \tag{41}$$

$$\mathcal{N}_\pm = \frac{R}{\lambda}\frac{\int_{-\alpha}^{\alpha} d\theta_w [f(\theta_w)]^2}{\int_{-\alpha}^{\alpha} d\theta_s f(\theta_w)\Phi(R,\theta_w)}, \tag{42}$$

$$\langle l^2\rangle_\pm = -\frac{R}{\lambda}\frac{\int_{-\alpha}^{\alpha} d\theta_w f(\theta_w)\frac{\partial^2 f(\theta_w)}{\partial\theta_s^2}}{\int_{-\alpha}^{\alpha} d\theta_w f(\theta_w)\Phi(R,\theta_w)}. \tag{43}$$

Setting Eq. (40) as

$$\omega_{\lambda\pm}^2(k) = \omega_{\lambda\pm}^2(0) - c_\lambda^2 k^2 \tag{44}$$

one finds that phonons are stable provided that $k^2 < k_\lambda^2$ with a threshold

$$k_\lambda^2 = \frac{\omega_{\lambda\pm}^2(0)}{c_s^2 + c_\lambda^2} \tag{45}$$

that vanishes in an incompressible fluid, whereas ripplons are the stable mode for higher wave number.

To perform numerical estimates one has to introduce an adequate representation of the substrate potential $U(r_w, \theta_w)$. In prior works[14,23,24] the simplest assumption has been that of adding the potentials of two planar surfaces meeting at an angle equal to the wedge opening. A more sophisticated and precise construction of the potential did not give rise to any substantial modification in the adsorption patterns of helium in alkali wedges;[25] accordingly, for the sake of a semiquantitative comparison of frequencies in the frame of the variational approach it is sufficient to adopt the simple prescription, employing the planar Cs potentials of Ref. 26.

Calculations carried in this way show that for sufficiently large samples and apertures above a few degrees the effective gravity is positive except for a narrow interval near the filling angle. The stability edges, Eq. (45), are shown in Fig. 6 for several l values, indicating that ripplons are the preferred mode except for very low wave numbers—almost vanishing on convex surfaces—and the only undamped excitations on interfaces of almost vanishing curvature, i.e., in the vicinity of the planar meniscus.

V. SUMMARY

This work contains the first estimates of the low-energy excitation spectrum of superfluid helium in a wedge. The formalism is adequate for samples of fluid large enough to secure the identification of a macroscopic contact angle; this

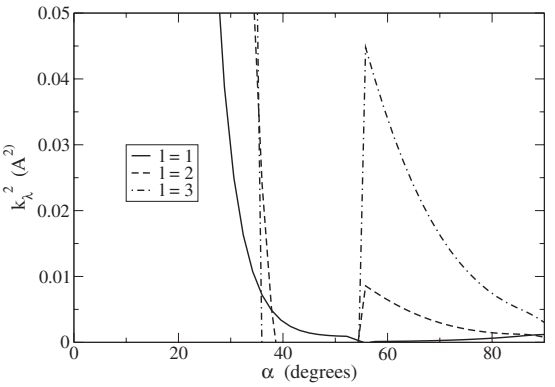

FIG. 6. Upper edges of phonon stability (in Å^{-2}) as functions of wedge opening for several values of the parameter l.

excludes the formation of bridges and concentrates the discussion on the crossover from concave meniscii at small wedge openings to convex surfaces at large angles, through a filling transition where the fluid exhibits a flat meniscus. The geometry permits a variational estimate of the oscillation frequencies, which suffices to examine the appearance of first and of third sound, and to establish the stability regimes of either mode in terms of the relevant parameters.

The wedge geometry and associated breaking of cylindrical symmetry introduces an ambiguity as to the choice of coordinates and quantization numbers for the spectrum. The wedge coordinates are the most adequate to satisfy the boundary condition at the substrate walls, at the price of complicating the construction of the dispersion relation based on the boundary condition at the free surface. In spite of the nonexistence of a quantization number associated with angular momentum, it is possible to recognize an orbital parameter playing the role of a quasiangular momentum and to assign a multipolarity to the modes for the sake of a classification. It is interesting that the variational dispersion relations obtained in this way bear a close resemblance to those for adsorbed shells in a cylindrical pore.[17]

The results here presented should provide a reference for future numerical calculations carried, for instance, in the current frame—appealing to a refined resolution of the spectrum beyond the variational estimate—or within a random-phase-approximation scheme, halfway between phenomenology and elaborated many-body techniques.

ACKNOWLEDGMENTS

This work was performed under Grant No. X099 from University of Buenos Aires and PICT 31980/05 from National Agency for the Promotion of Science and Technology of Argentina.

[1] E. Cheng and M. W. Cole, Phys. Rev. B **41**, 9650 (1990).
[2] E. H. Hauge, Phys. Rev. A **46**, 4994 (1992).
[3] M. Napiórkowski, W. Koch, and S. Dietrich, Phys. Rev. A **45**, 5760 (1992).
[4] P. Concus and R. Finn, Phys. Fluids **10**, 39 (1998).
[5] K. Rejmer, S. Dietrich, and M. Napiorkowski, Phys. Rev. E **60**, 4027 (1999).
[6] A. O. Parry, C. Rascón, and A. J. Wood, Phys. Rev. Lett. **83**, 5535 (1999).
[7] A. O. Parry, C. Rascón, and A. J. Wood, Phys. Rev. Lett. **85**, 345 (2000).
[8] C. Rascón and A. O. Parry, J. Chem. Phys. **112**, 5175 (2000).
[9] C. Rascón and A. O. Parry, Nature (London) **407**, 986 (2000).
[10] A. O. Parry, A. J. Wood, E. Carlon, and A. Drzewiński, Phys. Rev. Lett. **87**, 196103 (2001).
[11] L. Bruschi, A. Carlin, and G. Mistura, Phys. Rev. Lett. **89**, 166101 (2002).
[12] A. Milchev, M. Müller, K. Binder, and D. P. Landau, Phys. Rev. Lett. **90**, 136101 (2003).
[13] J. R. Henderson, Phys. Rev. E **69**, 061613 (2004).
[14] E. S. Hernández, F. Ancilotto, M. Barranco, R. Mayol, and M. Pi, Phys. Rev. B **73**, 245406 (2006).
[15] A. Hernando, E. S. Hernández, R. Mayol, and M. Pi, Phys. Rev. B **77**, 195431 (2008).
[16] F. Ancilotto, M. Barranco, E. S. Hernández, A. Hernando, and M. Pi, Phys. Rev. B **79**, 104514 (2009).
[17] W. F. Saam and M. W. Cole, Phys. Rev. B **11**, 1086 (1975).
[18] M. Barranco, E. S. Hernández, R. Mayol, and M. Pi, Phys. Rev. B **69**, 134502 (2004).
[19] F. Ancilotto, M. Barranco, E. S. Hernández, and M. Pi, J. Low Temp. Phys. **157**, 174 (2009).
[20] L. D. Landau and E. M. Lifshitz, *Fluid Mechanics* (Pergamon, Oxford, 1959).
[21] H. Lamb, *Hydrodynamics* (Dover, New York, 1993).
[22] T. Brooke Benjamin and J. C. Scott, J. Fluid Mech. **92**, 241 (1979).
[23] M. W. Cole, F. Ancilotto, and S. M. Gatica, J. Low Temp. Phys. **138**, 195 (2005).
[24] R. Mayol, F. Ancilotto, M. Barranco, E. S. Hernández, and M. Pi, J. Low Temp. Phys. **148**, 851 (2007).
[25] A. Hernando, E. S. Hernández, R. Mayol, and M. Pi, Phys. Rev. B **76**, 115429 (2007).
[26] A. Chizmeshya, M. W. Cole, and E. Zaremba, J. Low Temp. Phys. **110**, 677 (1998).